Kok, B., Forbush, B., & McGloin, M. (1970) *Photochem. Photobiol. 11*, 457-475.
Lavergne, J. (1987) *Biochim. Biophys. Acta 894*, 91-107.
Mathis, P., & Sêtif, P. (1981) *Isr. J. Chem. 21*, 316-320.
Metz, J. G., Nixon, P. J., Rögner, M., Brudvig, G. W., & Diner, B. A. (1989) *Biochemistry 28*, 6960-6969.
Michel, H., & Deisenhofer, J. (1988) *Biochemistry 27*, 1-7.
Murata, N., & Miyao, M. (1985) *Trends Biochem. Sci. 10*, 122-124.
Ono, T.-A., & Inoue, Y. (1988) *FEBS Lett. 227*, 147-152.
Ono, T.-A., & Inoue, Y. (1989) *Arch. Biochem. Biophys. 275*, 440-448.
Ono, T.-A., & Inoue, Y. (1990) *Biochim. Biophys. Acta 1020*, 269-277.
Ono, T.-A., Zimmermann, J.-L., Inoue, Y., & Rutherford, A. W. (1986a) *Biochim. Biophys. Acta 851*, 193-201.
Ono, T.-A., Conjeaud, H., Gleiter, H., Inoue, Y., & Mathis, P. (1986b) *FEBS Lett. 203*, 215-219.
Rutherford, A. W. (1989) *Trends Biochem. Sci. (Pers. Ed.) 14(6)*, 227-232.
Rutherford, A. W., Zimmermann, J.-L., & Boussac, A. (1992) in *The photosystems: Structure, function and molecular biology* (Barber, J., Ed.) Elsevier, New York (in press).
Satoh, K., & Katoh, S. (1985) *FEBS Lett. 190*, 199-203.
Saygin, Ö., Gerken, S., Meyer, B., & Witt, H. T. (1986) *Photosynth. Res. 9*, 71-78.
Sinclair, J. (1984) *Biochim. Biophys. Acta 764*, 247-252.
Sivaraja, M., Tso, J., & Dismukes, G. C. (1989) *Biochemistry 28*, 9459-9464.
Theg, S. M., Jursinic, P. A., & Homann, P. H. (1984) *Biochim. Biophys. Acta 766*, 636-646.
Theg, S. M., Filar, L. J., & Dilley, R. A. (1986) *Biochim. Biophys Acta 849*, 104-111.
Vass, I., & Styring, S. (1991) *Biochemistry 30*, 830-839.
Vass, I., Ono, T.-A., & Inoue, Y. (1987) *Biochim. Biophys. Acta 892*, 224-235.
Velthuys, B. R. (1988) *Biochim. Biophys. Acta 933*, 249-257.
Vermaas, W. F. J., Rutherford, A. W., & Hansson, Ö. (1988) *Proc. Natl. Acad. Sci. U.S.A. 85*, 8477-8481.
Völker, M., Eckert, H.-J., & Renger, G. (1987) *Biochim. Biophys. Acta 890*, 66-76.
Waggoner, C. M., & Yocum, C. F. (1990) in *Current Research in Photosynthesis* (Baltscheffsky, M., Ed.) Vol. I, pp 685-688, Kluwer Academic Publishers, Dordrecht, The Netherlands.
Yerkes, C. T., & Babcock, G. T. (1981) *Biochim. Biophys. Acta 634*, 19-29.
Yocum, C. F. (1991) *Biochim. Biophys. Acta 1059*, 1-15.

Sequential Resonance Assignments of Oxidized High-Potential Iron–Sulfur Protein from *Chromatium vinosum*†

David G. Nettesheim,*,‡ Scott R. Harder,§ Benjamin A. Feinberg, and James D. Otvos‖
Department of Chemistry, University of Wisconsin—Milwaukee, Milwaukee, Wisconsin 53201
Received July 19, 1991; Revised Manuscript Received October 7, 1991

ABSTRACT: 2D NMR spectra of the high-potential iron–sulfur protein (HiPIP) from *Chromatium vinosum* have been used to obtain partial resonance assignments for the oxidized paramagnetic redox state of the protein. Sequence-specific assignments were made using NOESY and COSY spectra in H_2O and D_2O of the following backbone segments: Asn-5–Arg-33, Glu-39–Asp-45, Gly-55–Cys-63, Gly-68–Ala-78, and Leu-82–Gly-85. NOESY spectra with a spectral width wide enough to include the hyperfine-shifted resonances revealed numerous NOE contacts between these signals and those in the main envelope of the proton spectrum. With the aid of the X-ray crystal structure [Carter, C. W., Kraut, J., Freer, S. T., Xuong, N. H., Alden, R. A., & Bartsch, R. G. (1974) *J. Biol. Chem. 249*, 4212], these NOEs permitted seven of the nine hyperfine-shifted signals to be assigned to three of the cysteine residues liganded to the metal cluster (Cys-43, Cys-46, and Cys-77). The other two hyperfine-shifted signals produced no detectable NOEs to other resonances in the spectrum and were tentatively assigned to the remaining cysteinyl ligand (Cys-63). These assignments, in conjunction with recent theoretical models of the electronic structure of the Fe_4S_4 cluster [Noodleman, L. (1988) *Inorg. Chem. 27*, 3677; Bertini, I., Briganti, F., Luchinat, C., Scozzafava, A., & Sola, M. (1991) *J. Am. Chem. Soc. 113*, 1237], indicate that the iron atoms coordinated to Cys-63 and Cys-77 are those of the mixed-valence Fe^{3+}–Fe^{2+} pair whereas Cys-43 and Cys-46 are ligands to the Fe^{3+}–Fe^{3+} metal pair.

Iron–sulfur proteins play important roles in terminal respiration, photosynthesis, and nitrogen fixation and are of particular structural interest because of the wide range of redox potentials they can adopt. Those containing one or more Fe_4S_4 clusters have the most complex electronic structures and are grouped into two classes according to their one-electron redox potentials and the $[Fe_4S_4]^{n+}$ core oxidation levels between which they interconvert ($n = +1/+2$ or $+2/+3$) (Palmer et al., 1975; Carter, 1977a). High-potential iron–sulfur proteins (HiPIPs) have relatively large positive reduction potentials of up to 350 mV and interconvert between the $+2/+3$ states while the low potential ferredoxins ($E°$ ca. −400 mV) shuttle between the $+1/+2$ states. Despite the existence of X-ray crystal structures for HiPIP from *Chromatium vinosum* (Carter et

† This research was supported by a grant to B.A.F. from the National Institutes of Health (GM 41927-01).
* To whom correspondence should be addressed.
‡ Present address: Abbott Laboratories D47G AP9, Abbott Park, IL 60064.
§ Present address: Nalco Chemical Co., Naperville, IL 60566.
‖ Present address: Department of Biochemistry, North Carolina State University, Raleigh, NC 27695.

0006-2960/92/0431-1234$03.00/0

al., 1974) and ferredoxin from *Peptococcus aerogenes* (Adman et al., 1973), it is still unclear how the polypeptide surrounding the cluster exerts its influence on the redox couple employed and the magnitude of the reduction potential.

To gain a better understanding of the electronic interactions between the Fe_4S_4 cluster and nearby residues of the protein, a number of ^1H NMR spectroscopic studies of HiPIPs have been conducted. In the earliest studies (Phillips et al., 1970), it was observed that oxidized HiPIPs exhibit a number of hyperfine-shifted peaks that are far downfield from the main spectral envelope of the protein. Spectra of reduced HiPIPs were also found to contain hyperfine-shifted signals that were fewer in number and located less far downfield than those in the oxidized protein. By comparison with spectra of several synthetic analogues of the Fe_4S_4 cluster (Holm et al., 1974; Que et al., 1974; Reynolds et al., 1978), it was suggested that the isotropic shifts are predominantly contact in origin and originate from protons of the cysteine ligands to the cluster. In a previous communication (Nettesheim et al., 1983), we reported that the chemical shift patterns and temperature and pH dependences of the hyperfine-shifted resonances of oxidized and reduced HiPIPs from *C. vinosum* and *Rhodopseudomonas gelatinosa* are very similar. Moreover, spectra of the oxidized proteins were found to contain three resonances that had not previously been detected, one at very low field (ca. 110 ppm) and two at very high field (ca. −30 ppm). Resonances in similar positions have more recently been found in HiPIPs isolated from four other species of photosynthetic bacteria (Krishnamoorthi et al., 1986, 1989; Sola et al., 1989), suggesting that this chemical shift pattern may be common to all HiPIPs. An exception is the HiPIP isolated from *Ectothiorhodospira halophila*, whose spectrum contains four, rather than two, upfield signals (Krishnamoorthi et al., 1986). Possibly related to this observation is the fact that the reduction potential of the protein is only 50 mV, which is much more negative than those of the other HiPIPs examined by ^1H NMR.

The prospects for reaching a better understanding of the relationship between HiPIP structure and the electronic properties of the Fe_4S_4 cluster, and the influence the cluster has on the ^1H NMR parameters of the protein, have been significantly enhanced by two recent developments. First, theoretical models for the oxidized Fe_4S_4 cluster have been proposed (Noodleman, 1988; Bertini et al., 1991) that successfully account for Mossbauer evidence for two distinct pairs of Fe sites, an Fe^{3+}–Fe^{3+} pair and a mixed-valence Fe^{3+}–Fe^{2+} pair (Papaefthymiou et al., 1986; Middleton et al., 1980; Antanaitas & Moss, 1975). Second, eight of the nine hyperfine-shifted resonances in the ^1H spectrum of oxidized *C. vinosum* HiPIP have been assigned on the basis of steady-state NOE experiments to the four pairs of geminal β-CH_2 cysteinyl protons (Cowan & Sola, 1990). Similar studies have provided the pairwise assignments of the β-cysteinyl protons in the reduced protein, and two-dimensional (2D) chemical exchange studies have established the connectivities between the hyperfine-shifted signals in the reduced and oxidized proteins (Bertini et al., 1991). The new theoretical model of the oxidized Fe_4S_4 cluster is able to account not only for the unusual upfield shifts seen for some of the cysteinyl protons in HiPIPs but also for the observed existence of both Curie-type and anti-Curie-type temperature dependences (Bertini et al., 1991).

Despite the advances made in relating the electronic structure of the HiPIP cluster to the NMR properties of its cysteinyl ligands, it will be difficult to make much further progress without sequence-specific assignments of the hyperfine-shifted resonances. By knowing which resonances arise from which cysteine residues in the protein, it will be possible for the first time to identify which Fe atoms in the cluster correspond to the mixed-valence and ferric ion pairs. This knowledge coupled with the detailed structural information available from the X-ray structure of HiPIP might then be expected to provide insights into the structural features of the surrounding polypeptide that modulate the electronic properties of the cluster.

In this paper, we present 2D NMR data that permit sequence-specific assignments to be made of all of the hyperfine-shifted resonances in oxidized HiPIP from *C. vinosum*. The job was made difficult by the paramagnetism of the iron cluster, which causes severe line broadening and T_1 relaxation rate enhancement of resonances of nearby protons, including those of all of the cysteine residues. We were able to overcome this problem by using an approach pioneered by La Mar and co-workers (McLachlan et al., 1988; Emerson & La Mar, 1990) in which 2D NOE data were used in conjunction with the X-ray crystal structure to extend sequence-specific assignments made in regions of the protein relatively far from the cluster to residues closer to the cluster.

Experimental Procedures

The isolation of *C. vinosum* HiPIP was carried out as described by Bartsch (1971, 1978). All NMR samples were dissolved in 30 mM sodium phosphate buffer. Samples in D_2O were prepared by lyophilizing and redissolving the protein in 99.9% D_2O. Samples dissolved in H_2O contained 10% D_2O. Protein concentrations were about 3 mM. Oxidized HiPIP samples were prepared by adding a 100% molar excess of $K_3Fe(CN)_6$ to the reduced protein after lyophilizing. T_1 relaxation measurements were obtained using the inversion–recovery method.

Phase-sensitive COSY and NOESY 2D data sets were collected with standard pulse sequences (Jeener et al., 1979) and phase programs and were acquired in the hypercomplex mode (Muller & Ernst, 1979; States et al., 1982). A relayed-COSY spectrum in H_2O in the absolute value mode (Wagner, 1983) was used to help identify the spin systems of side chains. All data were acquired at 500 MHz using a General Electric GN500 spectrometer equipped with a 1280 Nicolet computer. COSY and NOESY spectra acquired in 90% H_2O were obtained at both 12 and 25 °C. All 2D data sets consisted of 1K complex points in the t_2 dimension and 256 complex points in the t_1 dimension zero-filled to 1K. Solvent suppression of water was carried out by low-power irradiation during the relaxation time of both NOESY and COSY spectra and also during the mixing time of NOESY spectra. All NOESY spectra were acquired with a 100–125-ms mixing time except for those whose sweep widths were expanded to include the hyperfine-shifted resonances, in which case a 10-ms mixing time was used. All 2D NMR spectra were acquired with a 1-s relaxation delay, except for the 10-ms NOESY data sets, which used a 0.5-s delay. All 2D data sets were processed on a Silicon Graphics IRIS 4D/70G using the FTNMR program provided by Dr. Dennis R. Hare. All NOESY data sets were first baseline corrected by multiple linear baseline corrections in the t_2 dimension after the first Fourier transformation but prior to transformation in the second dimension. They were further baseline corrected by a fifth-order polynomial in the t_1 dimension after both Fourier transformations. All data were digitally filtered prior to Fourier transformation using either skewed-shifted sine-squared window functions or a Gaussian transformation. All chemical shifts were referenced to the water signal, which was

Table I: NMR Properties of the Hyperfine-Shifted Resonances at pH 7.0

signal	chemical shift (ppm) 35 °C	15 °C	5 °C	T_1[a] (ms)	T_2[a] (ms)	assignment[b]	Fe_r[c] (Å)	Δppm/ΔpH[d]
C1		112.15	117.33	6.1	1.3	Cys-63 HB2	4.0	1.31
C2	37.77	40.95	41.97	14.6	1.9	Cys-77 HB1	4.1	1.69
C3	35.30	38.17	39.51	2.8	0.6	Cys-63 HB1	3.2	0.98
C4	29.19	30.96	31.36	7.2	1.3	Cys-77 HB2	3.0	1.00
C5	26.51	27.91	28.52	47.8	5.5	Cys-77 HA	4.9	0.24
C6	25.43	23.76	23.32	7.8	1.6	Cys-46 HB1	3.4	−2.10
C7	24.90	23.41	23.08	7.0	1.2	Cys-46 HB2	3.1	−2.09
C8	−30.44	−40.29	−44.20	12.5	1.1	Cys-43 HB2	2.9	−3.75
C9	−32.63	−37.83	−39.82	28.5	2.9	Cys-43 HB1	4.0	−1.99

[a] Relaxation measurements were made at 15 °C. T_2 values were determined from the line width ($\Delta\nu_{1/2}$) and the relation $T_2 = 1/(\pi\Delta\nu_{1/2})$. [b] All assignments were based on NOE data except for C1 and C3, which were assigned to Cys-63 by elimination. Stereospecific assignments for Cys-63 were determined by assigning the proton closest to the iron–sulfur cluster to the resonance with the smaller T_1 value. [c] Fe_r is the distance between the assigned proton and the nearest Fe atom. [d] Δppm/ΔpH is the change in chemical shift observed upon protonation of His-42 (Nettesheim et al., 1983). (Positive numbers denote downfield chemical shift change.)

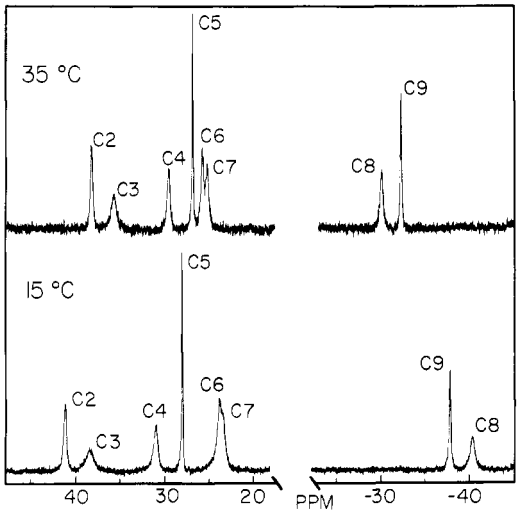

FIGURE 1: ^{1}H NMR spectra of oxidized HiPIP in D_2O, pH 7.0, at 15 and 35 °C. Only the spectral regions containing the hyperfine-shifted resonances are shown. Another hyperfine-shifted signal (C1) at about 110 ppm is not shown.

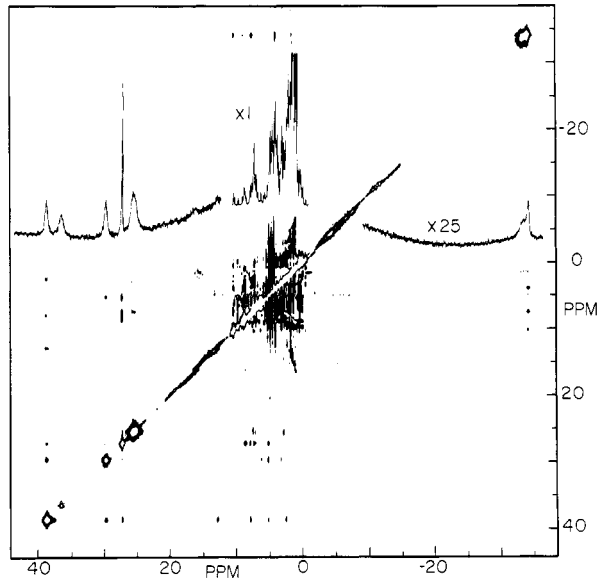

FIGURE 2: ^{1}H NOESY spectrum of oxidized HiPIP at 25 °C and pH 6.3 in D_2O. The spectral windows in both dimensions were set to include all hyperfine-shifted resonances shown in Figure 1. The mixing time was 10 ms.

assigned a value of 4.79 ppm at 25 °C and 5.02 ppm at 5 °C.

Proton distances were calculated from proton coordinates generated from the Brookhaven atomic coordinates of the X-ray crystal structure with the program FRODO. Stereospecific designations of protons are those used by the FRODO nomenclature.

Results

500-MHz ^{1}H NMR spectra of oxidized *C. vinosum* HiPIP are shown in Figure 1. Two upfield and six downfield hyperfine-shifted resonances can be seen with the spectral window used. There is an additional peak, signal C1, at about 110 ppm that is not shown (Nettesheim et al., 1983). To begin the process of assigning these signals, a 2D NOESY spectrum was acquired with a spectral width wide enough to include all of the hyperfine-shifted resonances except for that at 110 ppm (Figure 2). The resultant small dwell time at this wide sweep width produced severe distortions of the spectral baseline, which were removed by applying multiple linear baseline corrections to the spectra produced after the first transform in the t_2 dimension but before the second transform in the t_1 dimension. The mixing time used for this NOESY spectrum was by necessity only 10 ms because of the short T_1 values of the hyperfine-shifted resonances.

It can clearly be seen in Figure 2 that numerous NOE cross peaks were generated between the hyperfine-shifted resonances and those in the diamagnetic region of the spectrum. The only hyperfine-shifted resonance in this spectrum which fails to show any NOE cross peaks is C3, owing to its extremely short T_1 value of 2.8 ms (Table I). Resonance C5, on the other hand, has the longest T_1 and produces the most intense cross peaks. Some cross peaks were also observed between hyperfine-shifted resonances, namely, between signals C2 and C4 and between C2 and C5. These resonances have previously been assigned on the basis of 1D NOE experiments to the β-CH_2 protons of a single cysteine residue (C2 and C4) and tentatively to the α-proton of the same cysteine (C5) (Cowan & Sola, 1990). Other pairwise assignments to cysteinyl β-CH_2 protons made by these workers were resonances C1 and C3, C6 and C7, and C8 and C9.

Polypeptide Backbone Assignments. A partial assignment of the ^{1}H spectrum of oxidized HiPIP was accomplished by employing standard 2D NMR methodology to identify the through-bond and through-space connectivities along the backbone of the protein (Billeter et al., 1982; Wüthrich et al., 1982; Wüthrich, 1986). Because of the effects of the paramagnetic center on nearby residues, it proved very difficult to follow the connectivities along the polypeptide backbone as it neared the iron–sulfur cluster. The broad resonances of the cysteine protons that are shifted completely outside of the diamagnetic region of the spectrum do not present much problem, since they are well separated from other resonances. However, those protons experiencing a strong dipolar inter-

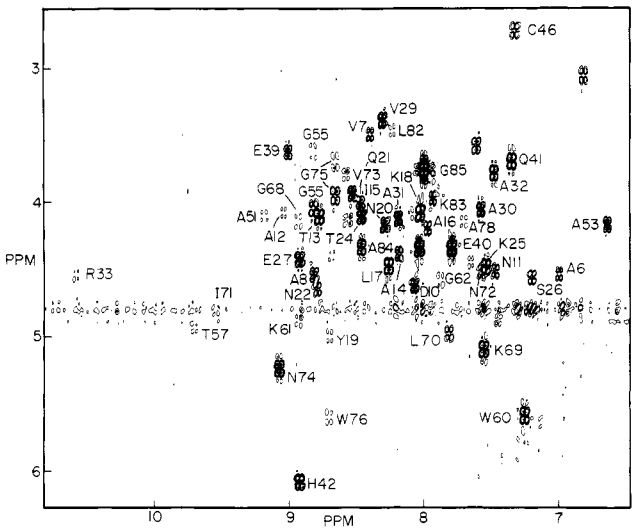

FIGURE 3: Fingerprint region of a COSY spectrum of oxidized HiPIP, at 25 °C and pH 7 recorded in 90% H_2O.

action with the paramagnetic center, but undergoing a relatively small contact shift, exhibit very broad resonances even though they are found in the normal 0–10 ppm region of the spectrum. NOE cross peaks from these resonances are very difficult to detect among those from their much sharper neighbors. Nevertheless, we were able to identify many of these resonances using classical sequence-specific assignment techniques.

The backbone fingerprint region of the COSY spectrum of oxidized HiPIP should contain a total of 85 cross peaks. At pH 7.0 and 25 °C, 56 cross peaks were observed in a COSY spectrum acquired in 90% H_2O (Figure 3). Additional cross peaks were seen in a COSY spectrum acquired at 12 °C in 90% H_2O and in COSY spectra from samples dissolved in D_2O. Altogether, we were able to observe a total of 65 COSY cross peaks in the fingerprint region. The missing cross peaks may have been lost owing to saturation transfer from irradiation of the H_2O signal or because their line widths were simply too large to produce a scalar cross peak of sufficient intensity to be seen. One of the COSY spectra acquired in D_2O contained quite a few amide proton signals even though the sample had been kept at room temperature for several days in D_2O before the spectrum was acquired. This fact proved to be fortunate since some of these nonexchanging amide protons are from residues deeply buried in the protein structure near the iron–sulfur cluster. The ability to resolve these resonances in D_2O samples was of critical importance for identifying several of the hyperfine-shifted resonances.

About 75% of the backbone amide ^1H's were able to be assigned in oxidized HiPIP. All spectra were acquired at pH 6.3 or higher. Although it would have been preferable to operate at a lower pH so as to take advantage of the slower exchange rate of amide protons with the solvent, the instability of the protein for long periods of time at lower pH precluded this. Figure 4 contains a summary of all the backbone NOEs of the assigned portion of oxidized HiPIP. The longest stretch to be identified was the segment running from Asn-5 to Arg-33 (Figure 5). d_{NN} cross peaks of varying intensities were discerned throughout this segment except where overlap prohibited distinguishing individual cross peaks. Small d_{NN} connectivities were usually accompanied by strong $d_{\alpha N}$ cross peaks between the same amino acids, although it proved much more difficult to resolve individual $d_{\alpha N}$ cross peaks because of chemical shift overlap in the fingerprint region of the spectrum. Strong $d_{\alpha N}$ NOEs were seen from Ala-6 to Ala-9,

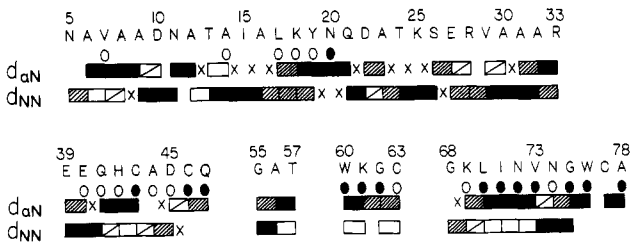

FIGURE 4: Sequential connectivities established for oxidized *C. vinosum* HiPIP. Only assigned segments of the amino acid sequence are shown. Strong cross peaks are marked with a solid bar, moderate to strong cross peaks with a hatched bar, moderate to weak cross peaks with a single diagonal, and weak cross peaks with an open bar. Those amide protons that exchange very slowly (longer then 24 h at 25 °C) are marked with a filled oval. An open oval indicates an intermediate exchange rate (long enough to be observed in a 12-h NOESY spectrum at 15 °C).

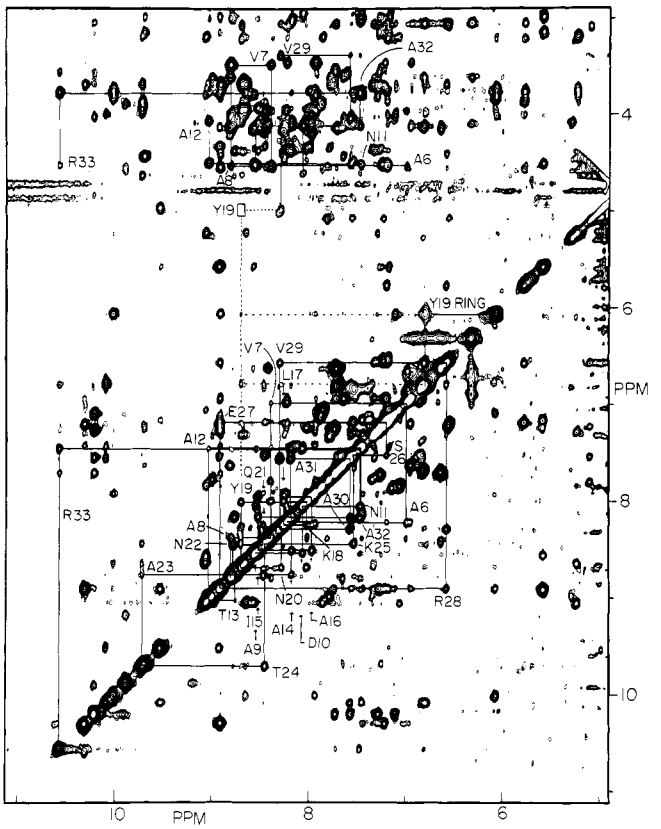

FIGURE 5: Section of a NOESY spectrum of oxidized HiPIP, 25 °C, pH 7.0 in 90% H_2O. The mixing time was 125 ms. d_{NN} connectivities are shown for the amino acid segments A6–A8 and A9–R33. Several selected $d_{\alpha N}$ connectivities are also traced out for this same region of the protein. The location of the scalar cross peak of Tyr-19 observed in the fingerprint region of the COSY spectrum in Figure 3 is marked with an open rectangle.

corresponding to an extended conformation found in the crystal structure. This section was followed by a short turn that resulted in first a strong d_{NN} and then a strong $d_{\alpha N}$ NOE from Asp-10 to Ala-12. Thr-13–Ala-16 produced a small stretch of strong d_{NN} NOEs that corresponded well to a small α-helical segment observed in the X-ray crystal structure. Residues Lys-18–Gln-21 produced small to moderate $d_{\alpha N}$ cross peaks accompanied by moderate d_{NN} NOEs. This segment in the crystal structure runs parallel to residues Ala-78–Gly-75, which are interposed between it and the cluster (Figure 11). Stronger $d_{\alpha N}$ NOEs might therefore have been expected from this region, but there was apparently significant attenuation of the Leu-17 and Tyr-19 α-CH proton signals owing to their close proximity to the saturated water resonance. This region of

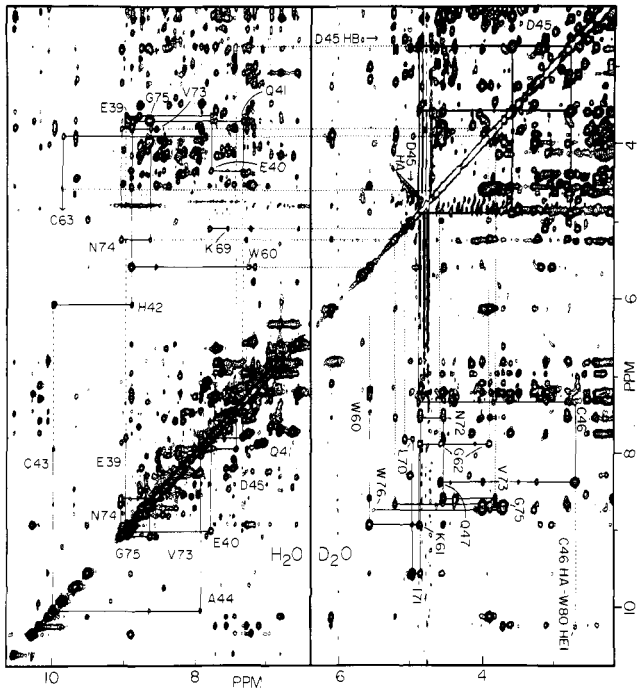

FIGURE 6: NOESY spectra of oxidized HiPIP, at 25 °C, pH 7.0. The spectrum in the left panel was acquired in 90% H_2O with a mixing time of 125 ms. The spectrum in the right panel was acquired in D_2O with a mixing time of 100 ms. Sequential $d_{\alpha N}$ connectivity data from both the H_2O and D_2O NOESY data sets along with d_{NN} connections are traced out for the sequences E39–Q47, W60–C63, and K69–W76.

the protein is of particular significance because of the importance attributed to Tyr-19 by several workers (Solo et al., 1989; Krishnamoorthi et al., 1986). Fortunately, it could be studied in more detail in a NOESY spectrum recorded at 15 °C immediately after dissolving lyopholized protein in D_2O (Figure 7), since the amide protons from Leu-17 to Asn-20 all exchange relatively slowly. Moderate to strong cross peaks were produced for both $d_{\alpha N}$ and d_{NN} connectivities, consistent with the extended structure observed in the crystal structure.

Continuing along the sequence, d_{NN} connectivities were found that agreed with a turn in the crystal structure from Ala-23 to Ser-26. This segment is followed by a small α-helical region running from Arg-28 to Ala-31 that produced a stretch of moderate to strong d_{NN} NOE cross peaks. The assignment process was able to be continued to Arg-33 but has not yet been extended to the following segment containing three proline residues. The assignments could be continued again starting at Glu-39 (Figure 6). As the polypeptide backbone approaches the iron–sulfur cluster (Figure 11), two strong d_{NN} NOEs followed by two strong $d_{\alpha N}$ NOEs are produced from Glu-39 to Cys-43. The strong $d_{\alpha N}$ cross peak produced by His-42 and Cys-43 is of particular importance because it establishes the identity of the amide proton of one of the four cysteines coordinated to the iron–sulfur cluster. The α-CH proton of Cys-43 could not be found. Two more small d_{NN} connectivities were found for the Cys-43–Asp-45 segment. The d_{NN} contact between Asp-45 and Cys-46 could not be made because of chemical shift overlap with the indole ring resonances of Trp-60. However, a small $d_{\alpha N}$ cross peak near the water resonance could be seen between the α-CH proton of Asp-45 and an amide proton that has tentatively been assigned to Cys-46.

Two other segments of the polypeptide backbone that have been identified are from Trp-60 to Cys-63 and from Gly-68 to Ala-78 (Figure 6). Both of these segments participate in an antiparallel β-sheet structure that prevents rapid exchange of the amide protons. The presence of numerous $d_{\alpha N}$ cross peaks in the less crowded NOESY spectrum accumulated in D_2O assisted in making the assignments of these two segments. Figure 6 contains segments from two different NOESY experiments conducted in H_2O and D_2O. Lines drawn to show connectivities between adjacent amino acids span the two segments to show how both the D_2O and H_2O data sets were used to identify resonances in a crowded region of the spectrum. $d_{\alpha N}$ NOEs were produced from Trp-60 to the Cys-63 amide proton, which allowed the second cysteine amide proton in HiPIP to be identified. Assignments could not be continued beyond Cys-63. Like Cys-43, no COSY cross peak could be found for Cys-63 in the $d_{\alpha N}$ fingerprint region. The Cys-43 and Cys-63 α-CH protons are, respectively, 3.0 and 4.6 Å from the nearest iron atom in the cluster as calculated from the X-ray crystal structure. Their proximity to the paramagnetic center apparently resulted in sufficient line broadening to preclude detection of any scalar cross peaks.

$d_{\alpha N}$ NOE cross peaks were found along the entire segment from Lys-69 to Trp-76. Although it was difficult to distinguish all of these cross peaks in the H_2O spectrum owing to chemical shift overlap, many of these NOEs were clearly seen in the D_2O spectra since the amide protons of Leu-70, Ile-71, Asn-72, Val-73, Gly-75, and Trp-76 all exchanged slowly in D_2O. Assignment could not be extended to Cys-77, whose amide proton is calculated to be only 3.8 Å from the nearest iron atom.

Identification of Aromatic Residues. Trp-60 was the easiest aromatic residue to identify. The indole ring of Trp-60 is situated well away from the iron–sulfur cluster and has relatively sharp resonances. Several NOE cross peaks could be seen between the Trp-60 α-CH proton and its own indole ring.

Tyr-19 was identified by sequence-specific assignments of the polypeptide backbone coupled with a detailed comparison of the NOE data with the X-ray crystal structure of HiPIP. Because of the proximity of the aromatic ring to the metal cluster, no scalar cross peak from the ring protons could be identified in any of the COSY spectra. However, a strong NOE cross peak originating from a pair of ring protons of Tyr-19 was observed and is labeled in Figures 5 and 7. The cross peak is much broader in one dimension than the other, implying that the proton associated with the upfield portion of the cross peak is closer to the iron–sulfur cluster. Numerous NOEs were found to the downfield resonance but not to the much broader upfield peak. Some of the NOE contacts to the downfield resonance are labeled in Figure 7. In addition to intraresidue NOEs, several cross peaks were found to Ala-14 and Val-7. On the basis of the crystal structure, the above-mentioned downfield resonance can be assigned to one of the Tyr-19 δ-CH ring protons. The absence of cross peaks to the upfield resonance makes its assignment uncertain.

A similar analysis was used to identify Trp-76. In addition to NOEs to its own β-CH_2 protons, the indole ring protons of Trp-76 showed NOE cross peaks to Gln-41, His-42, Arg-28, and Ala-31, all of which conform to the X-ray structure. A tabulation of the NOE cross peaks labeled in Figure 7 are presented in Table II along with the corresponding distances calculated from the X-ray crystal structure. The identification of the Trp-76 spin system and the partial assignment of Tyr-19 were crucial for assigning several of the downfield hyperfine-shifted resonances.

The aromatic ring protons of Trp-80, Phe-48, and Phe-66 were more difficult to study because of chemical shift overlap and line broadening resulting from their proximity to the iron–sulfur cluster. Their assignments will not be presented

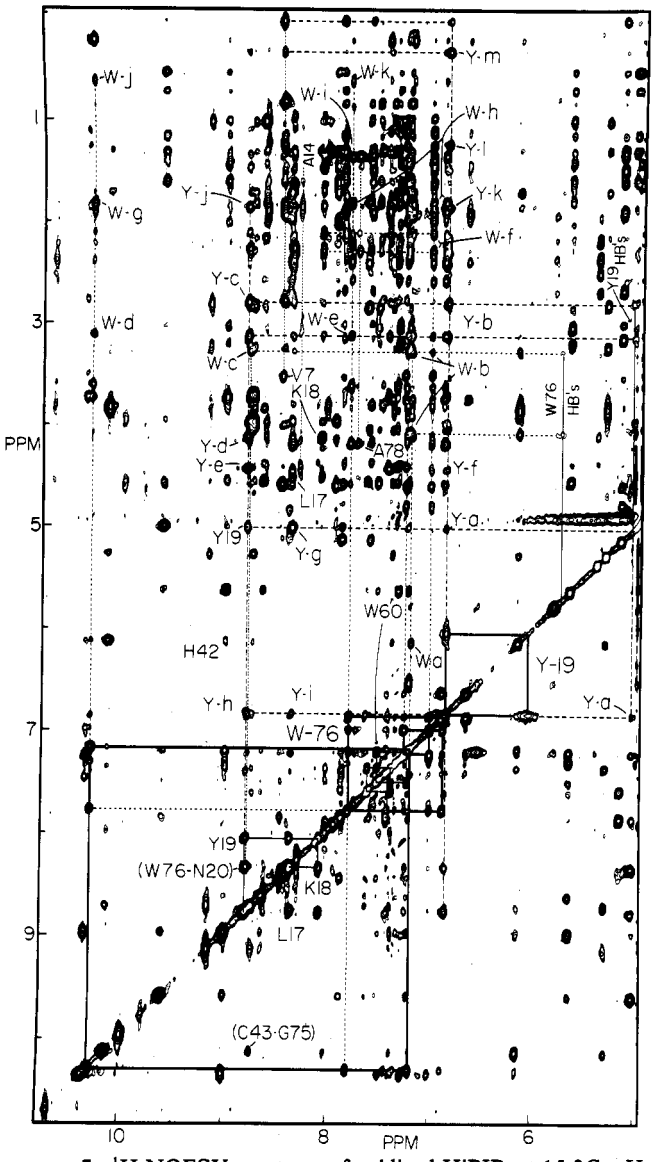

FIGURE 7: ^{1}H NOESY spectrum of oxidized HiPIP, at 15 °C, pH 7. The spectrum was acquired immediately after dissolving the sample in D_2O so as to observe as many slowly exchanging amide protons as possible. d_{NN} connectivities are traced out for L17–Y19. NOE cross peaks from Trp-76 and Tyr-19 have been labeled, respectively, with either W or Y. The distances calculated from the X-ray crystal structure for each labeled cross peak are listed in Table II.

here except for the indole-NH of Trp-80, which will be discussed later.

Identification of Hyperfine-Shifted Resonances. Seven of the hyperfine-shifted resonances were assigned by correlating the NOEs produced in the 10-ms NOESY spectrum to the higher resolution COSY and NOESY spectra used to assign the rest of the protein. A side-by-side comparison is shown in Figure 8 of the two small segments of the 10-ms NOESY spectrum containing the cross peaks of the downfield and upfield hyperfine-shifted resonances (panels A and C, respectively) and the 100-ms NOESY spectrum in D_2O (panel B). Resonances C2 and C4 were identified as the β-CH_2 protons of Cys-77 on the basis of NOEs observed between the two signals and resonances already assigned in the diamagnetic region of the spectrum. Resonance C2 gave NOEs to one of the Leu-17 β-CH_2 protons, the Tyr-19 α-CH, and the amide proton of Ala-78. C4 produced NOEs to the α-CH and one of the β-CH_2 protons of Tyr-19 and a third cross peak to one of the aromatic ring protons of Tyr-19. All of these NOE interactions are predicted by the X-ray structure and lend

Table II: NOE Contacts to Tyr-19 and Trp-76

label[a]	contact	interproton distance (Å)[b]
Y-a	Tyr-19 HD's–Tyr-19 HA	3.1, 4.3
Y-b	Tyr-19 HD's–Tyr-19 HB1	2.4, 3.7
	Tyr-19 HD's–Tyr-19 HB2	3.7, 2.4
Y-c	Tyr-19 HN–Tyr-19 HB1	2.9
	Tyr-19 HN–Tyr-19 HB2	2.2
Y-d	Tyr-19 HN–Lys-18 HA	2.9
Y-e	Tyr-19 HN–Ala-14 HA	3.4
Y-f	Tyr-19 HD's–Ala-14 HA	5.9, 3.8
Y-g	Tyr-19 HA–Asn-20 HN	2.2
Y-h	Tyr-19 HD's–Tyr-19 HN	5.1, 4.1
	Tyr-19 HD's–Trp-76 HN	3.2, 5.9
Y-i	Tyr-19 HD's–Asn-20 HN	3.3, 4.2
Y-j	Tyr-19 HN–Ala-14 HB	3.9
Y-k	Tyr-19 HD's–Ala-14 HB	6.3, 2.6
Y-l	Tyr-19 HD's–Val-7 HB	6.3, 4.3
Y-m	Tyr-19 HD's–Val-7 HH	5.5, 3.2
W-a	Trp-76 HD1–His-42 HA	2.8
W-b	Trp-76 HE3–Trp-76 HB2	2.6
	Trp-76 HD1–Trp-76 HB2	3.9
	Trp-76 HZ3–Trp-76 HB2	4.9
W-c	Trp-76 HN–Trp-76 HB2	3.0
W-d	Trp-76 HE1–Arg-28 HA	4.3
W-e	Trp-76 HZ2–Arg-28 HA	2.5
W-f	Trp-76 HZ3–Lys-18 HB2	3.2
W-g	Trp-76 HE1–Gln-41 HB2	2.2
W-h	Trp-76 HZ2–Ala-31 HB	2.7
	Trp-76 HH2–Ala-31 HB	2.4
W-i	Trp-76 HH2–Ala-78 HB1	3.9
W-j	Trp-76 HE1–Arg-28 HB1	3.2
W-k	Trp-76 HZ2–Arg-28 HB1	3.3

[a] The labels refer to the cross peaks identified in Figure 7. [b] Interproton distances calculated from the crystal structure.

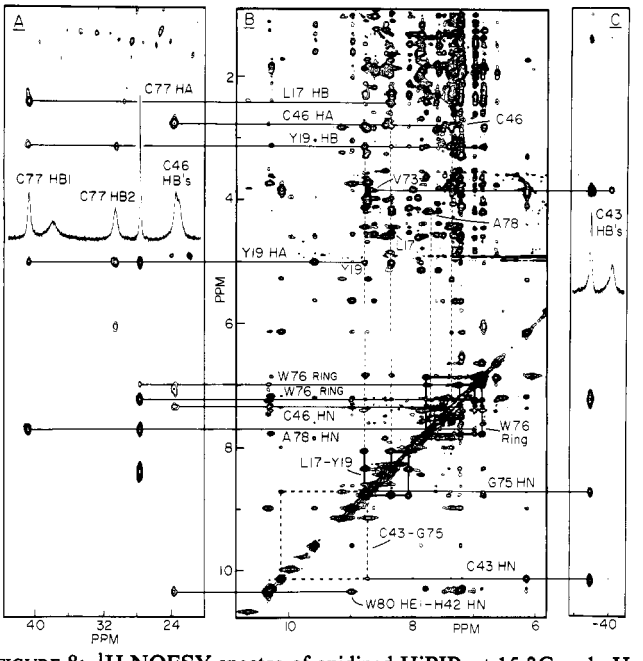

FIGURE 8: ^{1}H NOESY spectra of oxidized HiPIP, at 15 °C and pH 7 in D_2O. Panels A and C are the expanded regions of a 10-ms NOESY data set. The cross peaks in these two panels represent the NOEs produced between the hyperfine-shifted resonances and the ^{1}H signals in the diamagnetic region of the spectrum. The spectrum in panel B was produced by a higher resolution 100-ms NOESY experiment that does not include the hyperfine-shifted signals.

strong support to the assignment to Cys-77 β-CH_2 protons. The sharpest hyperfine-shifted resonance, C5, produced NOE cross peaks to the Tyr-19 α-CH, the indole ring proton of Trp-76, and the amide proton of Ala-78. All of these NOEs are consistent with the assignment of C5 to the Cys-77 α-CH proton. Figure 9 shows an expanded region of the 10-ms

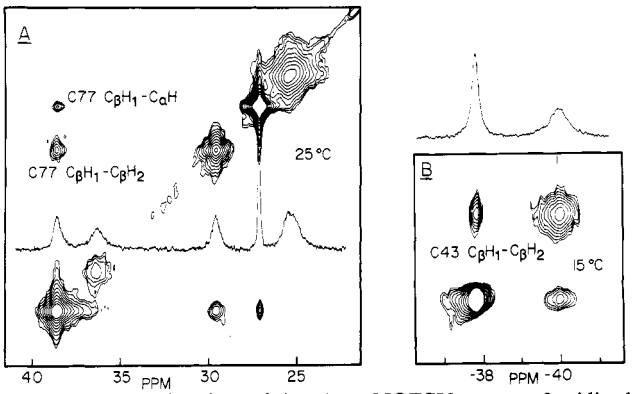

FIGURE 9: Selected regions of the 10-ms NOESY spectra of oxidized HiPIP at pH 7. Panel A is an expanded region of the downfield hyperfine-shifted resonances of a spectrum acquired at 25 °C. Panel B is an expanded region of the upfield hyperfine-shifted resonances from a spectrum acquired at 15 °C.

NOESY spectrum near the diagonal. In agreement with previous 1D NOE experiments (Cowan & Sola, 1990), cross peaks can clearly be seen between all three of these hyperfine-shifted resonances. The NOE interactions between these signals and those from neighboring residues that led to their assignment to Cys-77 are presented in the expanded view of this region of the protein structure given in Figure 10.

The upfield resonance C9 exhibited strong NOEs to the amide protons of Cys-43 and Gly-75 and to the α-CH proton of Val-73 (Figure 8). These NOE contacts are all consistent with the assignment of C9 to one of the Cys-43 β-CH_2 protons (Figure 10). The second upfield peak displayed a small NOE cross peak to the α-CH proton of Val-73, as well as a strong cross peak to C9 (Figure 9). On the basis of these two NOE interactions, C8 is assigned to the other member of the geminal pair of β-CH_2 protons of Cys-43.

Resonances C6 and C7 have been designated as the β-CH_2 protons of Cys-46 on the basis of NOE contacts from C6 to the α-CH and amide protons of Cys-46 and also to the Trp-80 indole-NH (Figures 8 and 10). Although resonance C6 produced a strong NOE cross peak to the signal assigned to Cys-46 α-CH, the latter assignment is itself somewhat tentative since only one weak NOE cross peak could be observed between Asp-45 and Cys-46. On the other hand, the Trp-80 indole-NH can readily be identified on the basis of expected NOEs deduced from the crystal structure, despite the fact that Trp-80 has yet to be assigned by classical sequence-specific techniques. A very strong NOE cross peak was observed between the His-42 amide proton signal and a resonance at about 10.3 ppm. The 10.3 ppm signal also produced small NOEs to Asp-45 and Gln-41 and, more importantly, a definite NOE to the hyperfine-shifted resonance C6. From an inspection of the X-ray crystal structure, these NOE contacts all conform with the assignment of the 10.3 ppm signal to the Trp-80 indole NH proton. Its NOE to resonance C6 in turn supports the assignment of C6 to one of the β-CH_2 protons of Cys-46. No cross peaks could be discerned between signals C6 and C7 because of the very small chemical shift separation between the two. However, the chemical shifts of both resonances exhibit anti-Curie temperature dependences (downfield shift with increasing temperature), and it can be safely assumed that they both belong to the same cysteine spin system (Bertini et al., 1991).

In an attempt to obtain additional support for the assignments of the hyperfine-shifted resonances made at pH 7.0, additional 2D NOESY experiments were conducted at pH 8.0 and 6.3. To improve the precision of the correlation of the

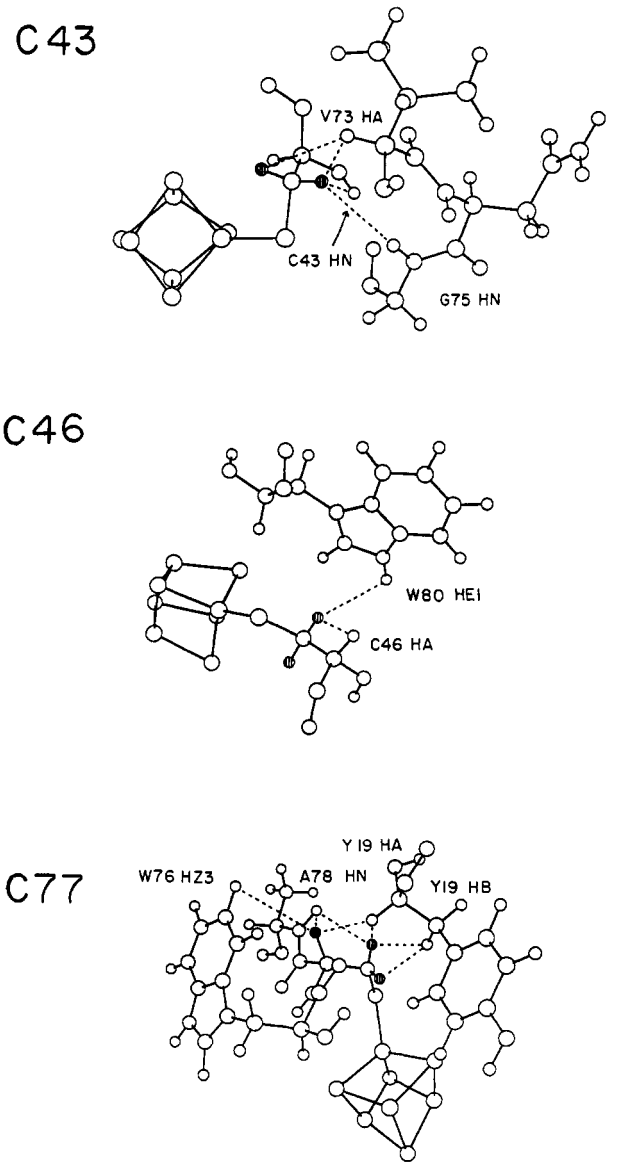

FIGURE 10: Structures of the immediate environments of three of the cysteine residues derived from the X-ray crystal structure of oxidized *C. vinosum* HiPIP. Some of the key NOEs expected from these structure are represented by dashed lines.

10-ms NOESY data set containing the hyperfine-shifted resonances to the higher resolution 125-ms NOESY spectrum, the 10-ms NOESY spectra were acquired with different dwell times. The dwell time in the second dimension was set so that the sweep width covered the whole spectral region containing the hyperfine-shifted resonances (about 45 000 Hz). The sweep width in the first dimension was adjusted so as to be the same as the 125-ms NOESY spectrum (8000 Hz), providing the same degree of resolution in that dimension. Although the digital filters would be expected to filter out the folded hyperfine-shifted resonances in the first dimension, they will have no effect on the cross peaks produced in the second dimension (Neuhaus & Williamson, 1989). Even though there was a loss in the signal-to-noise ratio of the pertinent NOE cross peaks in these higher resolution spectra, the data (not shown) clearly demonstrated that the chemical shifts of the cross peaks between the hyperfine-shifted resonances and those in the diamagnetic region responded to pH in the expected manner. These results greatly reduce the possibility that incorrect assignments were made because of chemical shift overlap. A summary of all assignments made in this work is given in Table III.

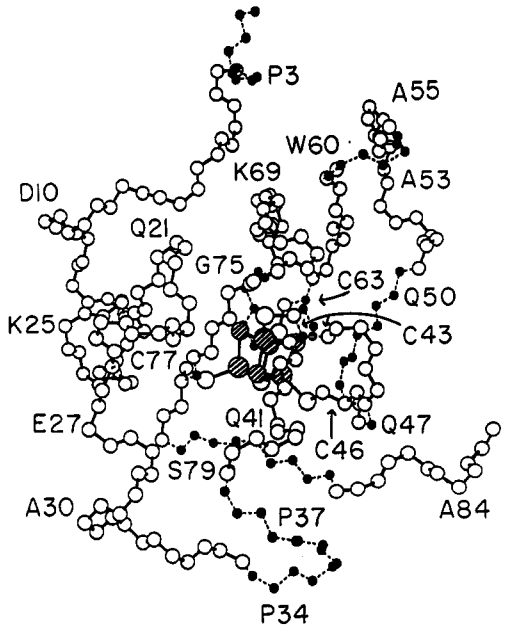

FIGURE 11: Structure of the polypeptide backbone of *C. vinosum* HiPIP generated from the X-ray crystal structure coordinates (Carter et al., 1974). Segments of the backbone that have been assigned are represented by large open circles and connected by solid lines. Unassigned segments are represented by small solid circles connected by dashed lines.

Discussion

Despite the complications associated with the presence of the paramagnetic center, it has been possible to assign all nine of the hyperfine-shifted resonances of oxidized *C. vinosum* HiPIP to protons of specific cysteine residues in the protein. This information provides the essential link between the high-resolution X-ray structure of HiPIP and the electronic properties of its Fe_4S_4 cluster as probed primarily by Mossbauer and magnetic resonance spectroscopies. The assignments were made solely on the basis of NOE interactions between the hyperfine-shifted signals and those protons of neighboring residues that were themselves identified by classical sequence-specific assignment methods and/or by correlating observed NOEs with those expected on the basis of the crystal structure. Because there is some danger of being misled by circular reasoning or the possibility that the crystal and solution structures are not identical, we have tried to be conservative and obtain as much corroborative NOE evidence as possible. As will be discussed below, the correctness of the cysteine assignments is supported by both T_1 relaxation data and the differential sensitivity of the resonance positions of the cysteine protons to pH.

The extent to which it was possible to assign the backbone protons of HiPIP is summarized in Figure 11, where large open circles connected by solid lines designate the backbone atoms whose protons were identified. As discussed by Carter et al. (1974), the HiPIP structure can be considered to consist of two domains. The carboxyl-terminal half of the molecule contains the ligands to the iron–sulfur cluster, while the amino-terminal domain consisting of residues 1–42 folds up upon the cluster binding segment. Since most of the amino-terminal segment is relatively distant from the iron–sulfur cluster, classical sequence-specific assignment techniques could be successfully applied. All amide protons in this domain were assigned except for two small segments (1–3 and 34–38) where the presence of proline residues broke up the continuity of peptide backbone NOEs. The carboxyl-terminal region was much more difficult to assign because of its proximity to the paramagnetic cluster. Fortunately, many of the amide protons near the cluster were resistant to solvent exchange, which made it possible to detect their broadened resonances once the signals of more rapidly exchanging protons were eliminated in D_2O solution. The stretch of residues from Lys-69 to Ala-78 was, in fact, one of the first to be assigned despite its proximity to the iron–sulfur cluster. This segment runs through the middle of the protein and participates in numerous hydrogen bonds which hinder amide proton exchange. The most difficult portions of the carboxyl-terminal domain to assign were those that are both near the cluster and relatively exposed to solvent. Most of the residues in these segments remain unassigned.

Among the hyperfine-shifted resonances, the easiest to assign were those exhibiting strong NOE interactions with protons located relatively far from the cluster. For example, the crystal structure indicates that one of the Cys-43 β-CH_2 protons (HB1) points away from the iron–sulfur cluster toward the surrounding polypeptide (Figure 10). Its resonance (C9) produces strong NOE cross peaks with those of Val-73 and Gly-75. On the other hand, the second Cys-43 β-CH_2 proton is directed toward the cluster and is near protons that are themselves near the paramagnetic center and presumably undergo efficient T_1 relaxation. Consequently, the only strong NOE cross peak that could be observed for this proton (C8) was to its own geminal proton (C9), with a weak cross peak to the α-CH proton of Val-73.

The Cys-77 spin system (signals C2, C4, and C5) produced the strongest NOE cross peaks and was identified without difficulty. Cys-77 is the only cysteine residue whose α-CH proton gives rise to a hyperfine-shifted resonance (C5) located outside the diamagnetic region of the spectrum. The reason for this is not obvious from the crystal structure. Cowan and Sola (1990) previously suggested that resonance C5 arises from the α-CH proton of Cys-43, solely on the basis of its close proximity to the iron–sulfur cluster and the assumption that the large hyperfine shift must be due to a dipolar contribution. In fact, the α-CH proton of Cys-77, which we have definitively assigned on the basis of NOE interactions, is the farthest cysteine α-CH proton from the cluster. It is therefore likely that the chemical shifts of the cysteine α-CH protons, like those of the β-CH_2 protons, are dominated by contact, rather than dipolar, interactions.

The resonances assigned to the β-CH_2 protons of Cys-46 (C6 and C7) have relatively short T_1 values (Table I) and produced relatively weak cross peaks. These are the only hyperfine-shifted resonances whose chemical shifts exhibit an anti-Curie temperature dependence (increased hyperfine shift with increasing temperature). Resonances C1 and C3 could not be assigned directly by NOE measurements since no NOE cross peaks could be detected to either signal. Both signals exhibit very short T_1 values (Table I), and resonance C1 is much farther from the diamagnetic region of the spectrum than the other downfield signals, which presents greater technical problems in acquiring good quality NOESY spectra. On the basis of the 1D NOE data of Cowan and Sola (1990) that clearly indicate that these signals are a geminal pair of cysteine β-CH_2 protons, they can be assigned with confidence to the remaining cysteine residue, Cys-63.

Indirect support for the assignments of the hyperfine-shifted resonances is provided by a reexamination of the pH dependence of their chemical shifts. As previously reported (Nettesheim et al., 1983), the ionization of the single histidine residue in the protein, His-42, exerts an influence on the shifts of all nine of the hyperfine-shifted signals. Examination of these data in the context of the proposed assignments reveals

Table III: Proton Resonance Assignments at pH 6.3 and 25 °C

residue	NH	αH	βH	others
Ser-1	–	–	–, –	
Ala-2	–	–		
Pro-3		–	–, –	–
Ala-4	8.80[a]	3.99	1.37	
Asn-5	8.21[a]	4.75	3.12, 2.66	
Ala-6	6.98	4.58	0.86	
Val-7	8.38	3.52	1.25	γH_3 0.35, 0.08
Ala-8	8.78	4.56	1.60	
Ala-9	8.53	4.15	1.49	
Asp-10	8.04	4.63	2.98, 2.57	
Asn-11	7.45	4.54	3.06, 2.92	
Ala-12	9.02	4.10	1.59	
Thr-13	8.74	4.13	4.41	γH_3 1.07
Ala-14	8.14	4.41	1.85	
Ile-15	8.50	3.96	1.92	γH_3 1.03; δH_3 0.92; γH 1.93, 1.22
Ala-16	7.94	4.22	1.64	
Leu-17	8.23	4.50	2.38, 2.22	γH 2.23; δH_3 1.26, 0.96
Lys-18	8.02	4.10	2.30, 2.11	–
Tyr-19	8.67	5.04	3.10, 2.78	δH 6.82[a]
Asn-20	8.29	4.18	2.34, 2.26	
Gln-21	8.47	4.01	2.27, 2.18	–
Asp-22	8.77	4.66	2.77, 2.41	
Ala-23	9.66[a]	3.89	1.67	
Thr-24	8.44	4.13	4.26	γH_3 1.30
Lys-25	7.52	4.49	2.12, 1.67	–
Ser-26	7.17	4.58	4.15, 3.78	
Glu-27	8.90	4.44	2.56, 1.89	–
Arg-28	6.56[a]	3.11	0.63, –0.66	–
Val-29	8.29	3.41	1.86	γH_3 0.96
Ala-30	7.56	4.07	1.43	
Ala-31	8.15	4.14	1.81	
Ala-32	7.45	3.81	1.37	
Arg-33	10.54	4.53	1.32, –	–
Pro-34		–	–, –	–
Gly-35	–	–, –		
Leu-36	–	–	–, –	–
Pro-37		–	–, –	–
Pro-38		–	–, –	–
Glu-39	9.00	3.64	1.99, 1.88	–
Glu-40	7.78	4.36	1.68, –	–
Gln-41	7.44	3.71	1.92, 1.82	γH 0.26, –0.17
His-42	9.00	6.16	4.03, 3.90	δH 7.56; ϵH 8.54
Cys-43	10.13[a]		–33.22,[a] –34.08[a]	
Ala-44	7.93[a]	3.85	1.23	
Asp-45	7.44	4.92	3.59, 2.76	
Cys-46	7.34	2.69	25.57,[a] 25.11[a]	
Gln-47	8.39	4.58	1.93, 1.78	–
Phe-48	–	–	–, –	–
Met-49	–	–	–, –	–
Gln-50	–	–	–, –	–
Ala-51	9.15	4.11	1.47	
Asp-52	8.40	4.74	2.78, 2.65	
Ala-53	6.62	4.19	1.30	
Ala-54	8.56	4.15	1.35	
Gly-55	8.79	4.06, 3.63		
Ala-56	7.63	4.47	1.64	
Thr-57	9.67	4.95	4.85	γH_3 1.42
Asp-58	–	–	–, –	
Glu-59	–	—	–, –	–
Trp-60	7.28	5.62	3.18, 3.02	NEH 10.18; H(2) 7.27; H(4) 7.19; H(5) 7.48; H(6) 7.34; H(7) 7.57
Lys-61	8.94	4.90	2.01, 1.58	–
Gly-62	7.89	4.62, 3.92		
Cys-63	9.96[a]		107.25,[a] 36.10[a]	
Gln-64	–	–	–, –	–
Leu-65	–	–	–, –	–
Phe-66	–	–	–, –	–
Pro-67		4.35	2.28, 1.96	–
Gly-68	8.90	3.78, 4.15		
Lys-69	7.56	5.12	1.89, 1.50	–
Leu-70	7.84	5.01	1.59, 1.16	γH 1.29; δH_3 0.72, 0.54
Ile-71	9.58	4.87	–, –	–
Asn-72	7.56	4.55	2.81, 1.79	
Val-73	8.60	3.82	2.16	γH_3 1.03, 1.00
Asn-74	9.18	5.25	3.22, 2.80	
Gly-75	8.70	4.00, 3.70		
Trp-76	8.76	5.56	4.02, 3.28	NEH 10.25; H(2) 7.11; H(4) 7.24; H(5) 6.99; H(6) 6.86; H(7) 7.76
Cys-77		27.00[a]	38.39,[a] 29.43[a]	

Table III (Continued)

residue	NH	αH	βH	others
Ala-78	7.77	4.15	1.35	
Ser-79	–	–	–, –	
Trp-80	–	–	–	NEH 10.26,[a] –
Thr-81	–	–	–	–
Leu-82	8.22	3.49	1.64, 1.38	γH 1.61; δH_3 1.24, 0.99
Lys-83	7.88	4.00	1.52, 1.13	–
Ala-84	8.45	4.36	1.36	
Gly-85	7.98	3.79, –		

[a] No scalar cross peaks could be found for these resonances in any COSY spectra. Their assignments are based solely on the NOE data.

a relationship between the magnitudes of the pH-dependent chemical shift changes and the distances of the cysteinyl protons to His-42. In the last column of Table I is given the total change in chemical shift observed for all nine hyperfine-shifted signals upon ionization of His-42. These values were obtained by a nonlinear least-squares fit of the chemical shift dependence on pH to a single ionization equilibrium. The resonances found to be most sensitive to pH are those attributed to the β-CH_2 protons of Cys-43 and Cys-46. These two cysteines are located on the same side of the iron–sulfur cluster as the imidazole ring of His-42, whereas Cys-63 and Cys-77 are on the opposite side of the cluster. The average pH-dependent chemical shift change for the β-CH_2 proton pairs of Cys-42, Cys-46, Cys-63, and Cys-77 are 2.87, 2.10, 1.15, and 1.34 ppm, respectively, while the corresponding distances between the imidazole ring of His-42 and the Fe atom coordinated to each cysteine are 10.3, 10.9, 12.6, and 12.4 Å. Thus, the magnitude of the influence of His-42 ionization on cysteine β-CH_2 chemical shift is clearly attenuated by distance, which is consistent with our previous conclusion that histidine protonation influences the iron–sulfur cluster via a direct electrostatic interaction rather than a conformational change (Nettesheim et al., 1983).

Another source of support for the NOE-based assignments of the cysteine protons is the good agreement found between the relative distances between these protons and the nearest iron atom of the cluster and their measured T_1 relaxation times. With the aid of the crystal structure, we have been able to make stereospecific assignments of the β-CH_2 protons of Cys-43, Cys-46, and Cys-77 on the basis of expected NOEs with neighboring protons (Table I). For example, resonance C2 was assigned as HB1 of Cys-77 on the basis of its strong NOEs to the β-CH_2 protons of Leu-17 and the Ala-78 amide proton, whereas signal C4 was designated HB2 owing to its strong NOE to the Tyr-19 α-CH proton (see Figure 10). Since the T_1 relaxation rates of the cysteine protons are expected to be dominated by dipolar, rather than scalar, interactions with the electron spin of the cluster, they would be predicted to exhibit an r^{-6} distance dependence, where r is the internuclear distance between the proton and the unpaired electron (Solomon, 1955; Gueron, 1975). As shown by the compilation of relaxation data and iron–proton distances in Table I, a good qualitative correlation is indeed observed between the T_1 values of each pair of cysteine β-CH_2 protons and the relative distances of these protons to the nearest iron center of the cluster. For each of the three cysteines for which NOE-based stereospecific assignments were made, the more distant HB1 proton was found to have a longer T_1 than its HB2 partner. The very long T_1 of signal C5 also is compatible with its assignment to the Cys-77 α-CH proton, which is farther from the cluster than any of the β-CH_2 protons.

The data in Table I indicate that the T_1 values of the HB1 and HB2 protons of Cys-77 and Cys-63 are much shorter than those of the corresponding protons of Cys-43, despite the fact they are virtually the same distances from the nearest iron atom. This observation is consistent with the existence of a significant degree of asymmetry in the distribution of the unpaired spin over the cluster, with relatively greater spin density residing in the vicinity of Cys-63 and Cys-77 and less in the vicinity of Cys-43. Such asymmetry has been demonstrated in other proteins containing paramagnetic metal centers and is a key feature of the emerging picture of the electronic structure of the HiPIP cluster (Bertini et al., 1991).

Another indication that the unpaired spin in oxidized HiPIP cannot be considered to be uniformly distributed over the cluster and onto its cysteine ligands comes from an analysis of the relationship of the cysteine hyperfine shifts to the Fe–S–C–H dihedral angles that, with the present assignments, can now be calculated from the X-ray structure. The large chemical shift dispersions observed for the contact-shifted resonances of cysteine β-CH_2 protons in iron–sulfur proteins have generally been attributed to variation of the dihedral angle ϕ between the Fe–S–C_β and S–C_β–H_β planes according to (Heller & McConnell, 1960; Poe et al., 1970)

$$A = B_0 + B_2 \cos^2 \phi$$

where A is the Fermi contact coupling constant, $B_2 \cos^2 \phi$ is the spin density transferred to the protons via a hyperconjugative mechanism, and B_0 is the spin density transferred by other mechanisms. Using our cysteine assignments, we obtained values for all of the relevant dihedral angles from the X-ray structure by computer graphics analysis and then used the above equation to assess its ability to predict the observed hyperfine shifts (assuming that B_0 is negligible compared to B_2). The results of this exercise were disappointing. Although the large chemical shift dispersion of the two β-CH_2 protons of Cys-63 was at least qualitatively consistent with their $\cos^2 \phi$ values, none of the chemical shift relationships among the other β-CH_2 proton pairs could be satisfactorily accounted for. Thus, in the present case, it does not appear that the hyperfine shifts can be explained simply on the basis of the angular orientation of the cysteine ligands. There are many possible reasons for this, among which are the participation of other mechanisms of spin delocalization besides hyperconjugation and a nonnegligible dipolar contribution to the hyperfine shifts.

With the sequence-specific assignments reported here for the hyperfine-shifted resonances of oxidized *C. vinosum* HiPIP, we come one step closer to an understanding of how the surrounding protein structure modulates the redox properties of the Fe_4S_4 core in iron–sulfur proteins. Recently proposed theoretical models of the electronic structure of the $[Fe_4S_4]^{3+}$ cluster (Noodleman, 1988; Bertini et al., 1991) are able for the first time to explain both its Mossbauer properties (Papaefthymious et al., 1986; Middleton et al., 1980; Antanaitas & Moss, 1975) and the complicated pattern of upfield and downfield ^1H NMR hyperfine shifts and their temperature dependences (Phillips et al., 1970; Nettesheim et al., 1983). The model considers the cluster, which formally consists of

three Fe^{3+} and one Fe^{2+} ions, to have electron density delocalized onto two specific pairs of iron atoms: an Fe^{3+}–Fe^{3+} pair with an $S = 4$ ground state and an Fe^{3+}–Fe^{2+} mixed-valence pair (equivalently $Fe^{2.5+}$) with an $S = 9/2$ ground state. It is the protons on the cysteine ligands to the mixed-valence pair of iron atoms that are predicted to give downfield hyperfine shifts and Curie-type temperature dependences (decreasing hyperfine shift with increasing temperature). Thus, our cysteine assignments of the resonances exhibiting this behavior (C1–C5) identify the iron coordinated to Cys-63 and Cys-77 as the mixed-valence pair, while those liganded to Cys-43 and Cys-46 are the ferric ion pair. Owing to antiferromagnetic coupling of the Fe^{3+} ions with the mixed-valence pair, the ferric pair of irons exhibits negative spin magnetization $\langle S_z \rangle$ and, under low-symmetry conditions, are predicted to give rise to the observed pattern of two upfield resonances (C8 and C9) and two downfield resonances (C6 and C7) with anti-Curie temperature dependences (under conditions of higher symmetry, the model predicts four upfield-shifted signals from the β-CH_2 protons of the cysteine ligands to the ferric pair, as is observed for HiPIP II from *Ectothiorhodospira vacuolata*).

With the identities now established of which metal ions in the crystal structure of *C. vinosum* HiPIP correspond to the two pairs of irons which give the protein its unique electronic properties, it will hopefully be possible in the near future to identify the specific structural interactions between polypeptide and cluster that are responsible for them.

ACKNOWLEDGMENTS

We thank Dr. Louis Noodleman for useful discussions regarding the electronic structure of HiPIP. We also thank Dr. Dennis Bennet for assisting with the molecular graphics.

Registry No. Cys, 52-90-4.

REFERENCES

Adman, E. T., Sieker, L. C., & Jensen, L. H. (1973) *J. Biol. Chem. 248*, 3987–3996.

Antanaitis, B., & Moss, T. (1975) *Biochim. Biophys. Acta 405*, 262–279.

Bartsch, R. G. (1971) *Methods Enzymol. 23*, 644–649.

Bartsch, R. G. (1978) *Methods Enzymol. 53*, 329–340.

Banci, L., Bertini, I., Luchinat, C., & Scozzafava, A. (1987) *J. Am. Chem. Soc. 109*, 2328–2334.

Banci, L., Bertini, I., & Luchinat, C. (1990) *Struct. Bonding (Berlin) 75*, 113–136.

Bertini, I., Briganti, F., Luchinat, C., & Scozzafava, A. (1990) *Inorg. Chem. 29*, 1874–1880.

Bertini, I., Briganti, F., Luchinat, C., Scozzafava, A., & Sola, M. (1991) *J. Am. Chem. Soc. 113*, 1237–1245.

Billeter, M., Braun, W., & Wüthrich, K. (1982) *J. Mol. Biol. 155*, 321.

Carter, C. W., Jr. (1977a) *Iron–Sulfur Proteins III* (Lovenberg, W., Ed.) pp 157–204, Academic Press, New York.

Carter, C. W., Jr. (1977b) *J. Biol. Chem. 252*, 7802–7811.

Carter, C. W., Jr., Kraut, J., Freer, S. T., Xuong, N. H., Alden, R. A., & Bartsch, R. G. (1974) *J. Biol. Chem. 249*, 4212–4225.

Cowan, J. A., & Sola, M. (1990) *Biochemistry 29*, 5633–5637.

Emerson, S. D., & La Mar, G. D. (1990) *Biochemistry 29*, 1545–1556.

Gueron, M. (1975) *J. Magn. Reson. 19*, 58–66.

Heller, C., & McConnell, H. M. (1960) *J. Chem. Phys. 32*, 1575.

Holm, R. H., Phillips, W. D., Averil, B. A., Mayerle, J. J., & Herskovitz, T. (1974) *J. Am. Chem. Soc. 96*, 2109–2117.

Jeener, J., Meier, B. H., Bachmann, P., & Ernst, R. R. (1979) *J. Chem. Phys. 71*, 4546.

Krishnamoorthi, R., & Markley, J. L. (1986) *Biochemistry 25*, 60–67.

Krishnamoorthi, R., Cusanovich, M. A., Meyer, T. E., & Przysiecki, C. T. (1989) *Eur. J. Biochem. 181*, 81–85.

McLachlan, S. J., La Mar, G. N., & Lee, K. B. (1988) *Biochim. Biophys. Acta 957*, 430–445.

Middleton, P., Dickson, D. P. E., Johnson, C. E., & Rush, J. D. (1980) *Eur. J. Biochem. 104*, 289–296.

Muller, L., & Ernst, R. R. (1979) *Mol. Phys. 38*, 963.

Nettesheim, D. G., Meyer, T. E., Feinberg, B. A., & Otvos, J. D. (1983) *J. Biol. Chem. 258*, 8235–8239.

Neuhaus, D., & Williamson, M. (1989) *The Nuclear Overhauser Effects in Structural and Conformational Analysis*, VCH Publishing Inc., New York.

Noodleman, L. (1988) *Inorg. Chem. 27*, 3677.

Palmer, G. (1975) *The Enzymes*, Vol XII, Part B, 3rd ed., pp 1–56, Academic Press, New York.

Papaefthymiou, V., Millar, M. M., & Munck, E. (1986) *Inorg. Chem. 25*, 3010–3013.

Phillips, W. D., Poe, M., McDonald, C. C., & Bartsch, R. G. (1970) *Proc. Natl. Acad. Sci. U.S.A. 67*, 683.

Poe, M., Phillips, W. D., McDonald, C. C., & Lovenberg, W. (1970) *Proc. Natl. Acad. Sci. U.S.A. 65*, 797–804.

Que, L., Jr., Anglin, J. R., Bobrik, M. A., Davison, A., & Holm, R. H. (1974) *J. Am. Chem. Soc. 96*, 6042–6048.

Reynolds, J. G., Laskowski, E. J., & Holm, R. H. (1978) *J. Am. Chem. Soc. 100*, 5315–5322.

Sola, M., Cowan, J. A., & Gray, H. B. (1989) *Biochemistry 28*, 5261–5268.

Solomon, I. (1955) *Phys. Rev. 99*, 559.

States, D. J., Haberkorn, R. A., & Reuben, D. J. (1982) *J. Magn. Reson. 48*, 286.

Wagner, G. (1983) *J. Magn. Reson. 55*, 151.

Wüthrich, K. (1986) *NMR of Proteins and Nucleic Acids*, Wiley, New York.

Wüthrich, K., Wider, G., Wagner, G., & Braun, W. (1982) *J. Mol. Biol. 115*, 311.